Dalton Transactions

Cite this: *Dalton Trans.*, 2011, **40**, 4599

www.rsc.org/dalton

PAPER

High-pressure synthesis and neutron diffraction investigation of the crystallographic and magnetic structure of $TeNiO_3$ perovskite

M. J. Martínez-Lope,[a] M. Retuerto,[a,b] J. A. Alonso,*[a] J. Sánchez-Benítez[a] and M. T. Fernández-Díaz[c]

Received 13th December 2010, Accepted 23rd February 2011
DOI: 10.1039/c0dt01752c

$TeNiO_3$ has been prepared under moderate pressure conditions (3.5 GPa), starting from a reactive TeO_2 and $Ni(OH)_2$ mixture contained in a sealed platinum capsule under the reaction conditions (850 °C for 2 h). The sample has been studied by neutron powder diffraction (NPD) data and magnetization measurements. $TeNiO_3$ crystallizes in an orthorhombically-distorted perovskite structure (space group P*nma*) with the unit cell parameters $a = 5.9588(1)$ Å, $b = 7.5028(1)$ Å and $c = 5.2143(1)$ Å. The NiO_6 octahedral network is extremely tilted, shaping a trigonal-pyramidal environment for the Te, where it is effectively coordinated to three oxygen atoms at Te–O distances of 1.92 Å. Below $T_N \approx 130$ K, it experiences an antiferromagnetic ordering, as demonstrated by susceptibility and NPD measurements. Above the Néel temperature, a paramagnetic moment of 3.24(1) μ_B/f.u. and $\theta_{Weiss} = -199(1)$ K are obtained from the reciprocal susceptibility. Below T_N, the magnetic reflections observed in the neutron patterns can be indexed with a propagation vector $k = 0$. The magnetic structure corresponds to the magnetic mode G_yF_z. The magnetic moments are oriented along the y-direction, with a canting along the z-axis. This ferromagnetic component explains the weak ferromagnetism observed in the magnetization isotherms; the infrequent shape of the magnetization cycles suggests a metamagnetic transition below 0.2 T. At $T = 2.5$ K, the ordered magnetic moment for the Ni^{2+} ions is 1.88(5) μ_B for the G_y mode and 0.9(2) μ_B for the F_x mode.

Introduction

Classical examples of perovskite ABO_3 oxides typically contain alkaline, alkaline-earth or rare-earth cations at the A positions, whereas the B sites are occupied by transition metals. Much less frequent are examples of perovskite oxides containing p-elements with an inert electron pair at the A positions, like Tl^+, Sn^{2+}, Sb^{3+}, Bi^{3+}, Se^{4+} or Te^{4+}. These cations have little volume and therefore their stabilization in perovskite-like oxides implies, in general, the use of high-pressure conditions.[1] Two paradigmatic examples are constituted by $SeCuO_3$[2] and $BiMnO_3$.[3] The structural distortion is so large that the superexchange Cu–O–Cu or Mn–O–Mn angles are very bent and favour ferromagnetic interactions, according to the Goodenough–Kanamori rules. For instance, in the $Se_{1-x}Te_xCuO_3$ series,[4] the magnetic interactions can be tuned between ferromagnetic for $SeCuO_3$, exhibiting tilting angles of the CuO_6 octahedra of $\phi = 121°$, and antiferromagnetic for $TeCuO_3$, with $\phi = 131°$, as demonstrated by magnetic susceptibility measurements. The effect of cationic substitutions at the B sublattice in the $Se(Cu_{1-x}Mn_x)O_3$ series[5] shows a sharp drop in the magnetization and a change from positive to negative Weiss constant upon Mn doping. Besides, the presence of a lone electron pair in the A cation induces cationic shifts that favour ferroelectricity; some of these materials are magneto-ferroelectrics, useful for multiple-memory devices (storage of information with both electrical and magnetic polarization) or memory elements in which a ferroelectric bit is read as a ferromagnetic bit generated by association.

On the other hand, whereas there are many examples of ABO_3 perovskites with valence combinations 1–5 (*e.g.* $LiNbO_3$), 2–4 (*e.g.* $SrTiO_3$) or 3–3 (*e.g.* $LaNiO_3$), very few examples of perovskites exhibiting a tetravalent state for the A cation and a divalent state for the B ion are known. This is, in part, due to the lack of tetravalent ions with the correct size to occupy A positions. Furthermore, the stabilization energy of the crystal structure is lower for an octahedral network of divalent cations. The only examples described so far of the 4–2 combination are the above-described perovskites that contain a p element at the A positions (Se^{4+}, Te^{4+}); the strong A–O covalent bonding and the lone electron pair that is able to fill the space of the A cation contribute to their structural stability. As mentioned before, these perovskite oxides can only be prepared under high-pressure conditions.

In this framework, we have recently prepared and studied $SeCoO_3$[6] and $SeMO_3$ (M = Ni, Mn)[7] oxides at moderate pressures of 3.5 GPa starting from very reactive precursors sealed in Pt capsules that underwent thermal treatments in moderate temperature conditions of the 700–850 °C range. The use of moderate pressure conditions allowed sufficiently large amounts of sample

[a]*Instituto de Ciencia de los Materiales de Madrid, CSIC, E-28049, Cantoblanco-Madrid, Spain. E-mail: ja.alonso@icmm.csic.es*
[b]*Department of Chemistry, Rutgers, State University of New Jersey, Piscataway, New Jersey, 08854-8087, USA*
[c]*Institut Laue-Langevin, B.P. 156, F-38042, Grenoble Cedex 9, France*

(≅ 0.5 g) to be prepared as required to perform neutron powder diffraction studies of their crystal and magnetic structures. All of these perovskite materials contain a network of extremely tilted octahedra, where the SeO_8 polyhedra are strongly distorted due to the presence of the electron lone pair of Se^{4+}, giving rise to effective $(SeO_3)^{2-}$ polyhedra. The strongly covalent Se–O bonds contribute to the stability of the $a^+b^-b^-$ tilt system of the MO_6 octahedral network. The same magnetic structure was observed for M = Ni and Mn below T_N = 104 K (M = Ni) and T_N = 53.5 K (M = Mn), defined by the propagation vector $k = 0$ and the basis vector $(0,0,A_z)$. It is a collinear antiferromagnetic arrangement of Ni^{2+} or Mn^{2+} spins lying along the c-direction, defined as G-type (P*bnm* setting). For $SeCoO_3$, the magnetic reflections were also indexed with a propagation vector $k = 0$, although the magnetic structure resulting was different: given by the basis vectors $(A_x,G_y,0)$ with Co^{2+} moments lying on the (a,b) plane of the perovskite; the structure being non-collinear but non-canted.

The aim of this paper is to report the synthesis, and the crystal and magnetic structures of $TeNiO_3$ perovskite, studied by neutron diffraction data complemented with susceptibility and magnetization measurements. $TeNiO_3$ has been previously described as an antiferromagnet with T_N = 125(2) K.[1]

Experimental

About 0.5 g of a stoichiometric mixture of TeO_2 and $Ni(OH)_2$ was thoroughly ground and put into a platinum capsule (6 mm diameter), sealed and placed in a cylindrical graphite heater. The reaction was carried out in a piston-cylinder press (Rockland Research Co.) at a pressure of 3.5 GPa at 850 °C for 2 h. The material was then quenched to room temperature in 5 s by the water-cooling system after switching off the power, and the pressure was subsequently released.

The product was initially characterized by laboratory XRD (Cu-Kα, λ = 1.5406 Å) for phase identification and to assess phase purity. For structural refinements, NPD patterns were collected at room temperature (295 K) with the high resolution D2B neutron diffractometer (ILL-Grenoble). In spite of the relatively small amount of sample available (about 0.5 g), due to the high-pressure synthesis procedure, a good quality pattern could be collected in high-flux mode and with a counting time of 4 h. A wavelength of 1.594 Å was selected from a Ge monochromator. Low temperature, medium-resolution NPD patterns were collected in the high-flux D20 diffractometer with λ = 2.40 Å in order to follow the thermal evolution of the magnetic structure. The sample was placed in an orange cryostat (standard cryostat used at ILL in the 1.5–350 K temperature range) and cooled down to 2.5 K. Sequential NPD diagrams were then collected during the heating run at 1.4 K min^{-1} in the 2.5–168.5 K temperature range, with a counting time of 4 min per diagram. All the patterns were refined with the Rietveld method[8] using the FULLPROF refinement program.[9] A pseudo-Voigt function was chosen to generate the line shape of the diffraction peaks. No regions were excluded in the refinement. In the final runs, the following parameters were refined: scale factor, background coefficients, zero-point error, unit cell parameters, pseudo-Voigt correction for asymmetry parameters, positional coordinates, isotropic thermal factors and the magnitude of the Ni magnetic moments. The coherent scattering lengths for Te, Ni and O were 5.80, 10.30 and 5.803 *fm*, respectively. The magnetic form factor considered for the Ni^{2+} cations was determined with coefficients taken from the International Tables of Crystallography.

The magnetic measurements were performed in a commercial superconducting quantum interference device magnetometer (SQUID). The *dc* magnetic susceptibility curve was obtained in the temperature range 1.8 < T < 300 K under a 1 kOe magnetic field. Magnetization isotherms were measured at T = 4, 100 and 300 K for magnetic fields ranging from –40 to 40 kOe.

Results

$TeNiO_3$ was obtained as a green polycrystalline powder. It is worth pointing out that the use of $Ni(OH)_2$ as a starting reactant seems to be crucial for the crystallization of the perovskite, perhaps because of water vapor transport-driven reactions. A hydrothermal-like reaction cannot be discarded, since the released water under these HP/HT conditions is a supercritical fluid. Previous trials with TeO_2 + NiO mixtures as starting reactants were unsuccessful, yielding mixtures of reactants with a minor perovskite phase. The XRD pattern (Fig. 1) is characteristic of a well-crystallized perovskite and can be indexed in an orthorhombic unit cell in the space group P*nma*. An impurity phase of NiO was detected in the $TeNiO_3$ pattern, as indicated in Fig. 1 with a star.

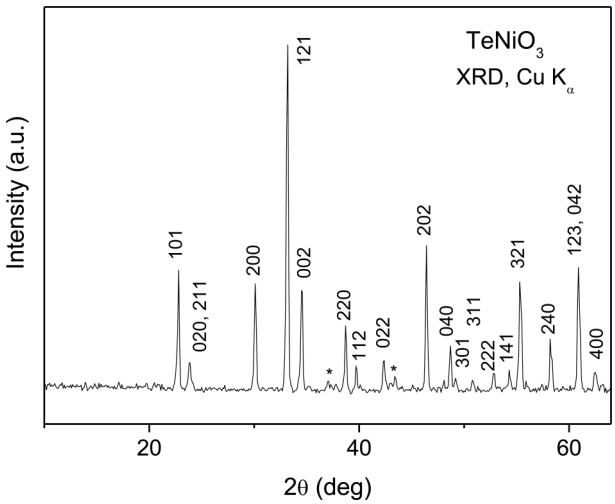

Fig. 1 XRD pattern of $TeNiO_3$ indexed in an orthorhombic unit cell with $a \approx c \approx \sqrt{2}a_0$, $b \approx 2a_0$ ($a_0 \approx 3.8$ Å). The star indicates the most intense reflections of the NiO impurity.

Crystallographic structure

The refinement of the crystallographic structure of $TeNiO_3$ was performed from an NPD pattern obtained at room temperature. The structure was defined in the orthorhombic space group P*nma* (no. 62), $Z = 4$, with unit cell parameters related to a_0 (ideal cubic perovskite, $a_0 \approx 3.8$ Å) as $a \approx c \approx \sqrt{2}a_0$, $b \approx 2a_0$. The structural parameters corresponding to $SeNiO_3$[7] were used as a starting model. Te atoms were located at 4c positions, Ni at 4b positions, and oxygen atoms at 4c and 8d positions, respectively. The oxygen stoichiometry at the O1 and O2 positions was checked by refining their occupancy factors; no oxygen vacancies were detected within the standard deviations. Both the XRD and NPD patterns showed

Table 1 Atomic parameters after the refinement of the crystallographic structure of $TeNiO_3$ from high resolution NPD data at $T = 295$ K. Space group P*nma*. Lattice parameters: $a = 5.9588(1)$, $b = 7.5028(1)$, $c = 5.2143(1)$ Å and $V = 233.116(8)$ Å^3. Discrepancy factors: $R_p = 2.50\%$, $R_{exp} = 2.57\%$, $R_{wp} = 3.22\%$ and $R_{Bragg} = 4.20\%$. $\chi^2 = 1.57$

Atom	Site	*x*	*y*	*z*	f_{occ}	*B*/Å^2
Te	4c	0.9857(7)	1/4	0.9815(8)	1.0	0.45(6)
Ni	4b	0	0	1/2	1.0	0.48(3)
O1	4c	0.0540(5)	1/4	0.3424(7)	1.01(2)	0.48(3)
O2	8d	0.1804(5)	0.0638(3)	0.8583(5)	0.98(2)	0.75(4)

the presence of extra reflections, which could be associated with a minor impurity of NiO. From the scale factors, 2.6(1)% of NiO was determined to be present in the sample. The good agreement between the observed and calculated NPD patterns is illustrated in Fig. 2. The lattice parameters obtained during the fitting and the reliability factors are included in Table 1. The unit cell parameters compare well with those given in Ref. 1: $a = 5.9564(3)$, $b = 7.4986(4)$ and $c = 5.2128(2)$ Å. The atomic positions determined in the structural refinement are also presented in Table 1. The atomic distances corresponding to the NiO_6 octahedra, the TeO_8 polyhedra and also some selected bonding angles are shown in Table 2. A view of the crystallographic structure of $TeNiO_3$ is illustrated in Fig. 3, highlighting the significant tilting of the NiO_6 octahedra.

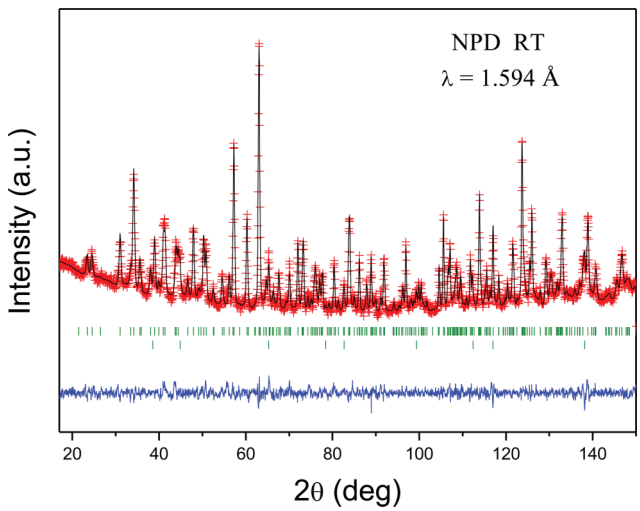

Fig. 2 Experimental (crosses) and calculated (solid line) NPD patterns collected with $\lambda = 1.594$ Å at room temperature; the difference profile is at the bottom. The first series of reflection markers corresponds to the main perovskite phase, the second to NiO.

Magnetic measurements

The thermal evolution of the magnetic susceptibility for $TeNiO_3$ is displayed in Fig. 4. There is a notable increase of the susceptibility below $T_N = 130$ K, indicating the onset of a magnetic ordering. The susceptibility tends to saturation at lower temperatures, with an intermediate inflexion at 40 K. The reciprocal susceptibility, displayed in the inset of Fig. 4, presents a linear behaviour above 150 K. A Curie–Weiss fit in the 150–300 K temperature range gives a paramagnetic temperature $\theta_w = -199(1)$ K and an effective paramagnetic moment of 3.24(1) μ_B. These figures are in

Table 2 Atomic distances (Å) for NiO_6 octahedra and TeO_8 polyhedra, and some selected bond angles (°) at 295 K

Ni–O1 (×2)	2.073(2)
Ni–O2 (×2)	2.208(3)
Ni–O2 (×2)	2.098(3)
<Ni–O>	2.126(3)
Te–O1	1.925(6)
Te–O1	2.731(5)
Te–O2 (×2)	1.926(4)
Te–O2 (×2)	2.898(5)
Te–O2 (×2)	2.687(3)
$<Te–O>_{3\ short}$	1.926(5)
Ni–O1–Ni	129.6(6)
Ni–O2–Ni	133.7(1)
<Ni–O–Ni>	131.66(8)
O1–Te–O2	101.5(3)
O2–Te–O2	93.0(2)

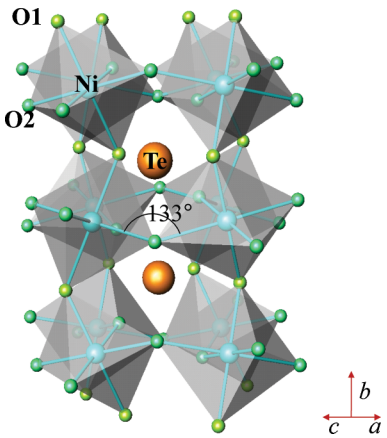

Fig. 3 A schematic view of the crystallographic structure of $TeNiO_3$; the NiO_6 octahedra are strongly tilted, giving rise to an irregular environment around Te cations (large spheres).

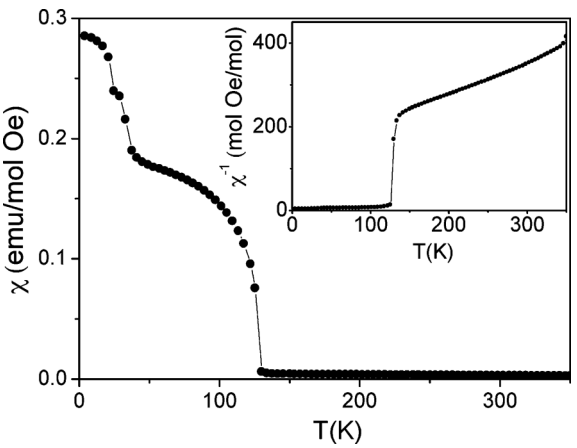

Fig. 4 Susceptibility *vs.* temperature plot for $TeNiO_3$. Inset: reciprocal susceptibility *vs.* temperature.

reasonable agreement with those previously reported for $TeNiO_3$,[1] $\theta_w = -270$ K and $m_{eff} = 3.4$ μ_B. For Ni^{2+}, with the electronic configuration $3d^8$ and ground state $^3F_4$, the theoretical effective magnetic moment (spin only) is 2.83 μ_B. This suggests a partially unquenched orbital moment for Ni^{2+}, given the relatively strong distortion of the NiO_6 octahedra. The isothermal magnetization curves of $TeNiO_3$ measured at $T = 4$, 100 and 300 K are shown

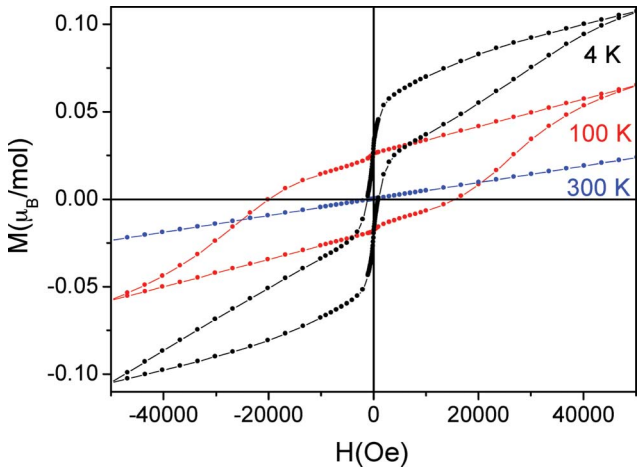

Fig. 5 Isothermal magnetization curves of $TeNiO_3$ obtained at $T = 4$, 100 and 300 K.

in Fig. 5. Below T_N, the presence of a wide hysteresis loop with a very small remnant magnetization, of around 0.06 μ_B/formula, suggests the presence of a weak ferromagnetism phenomenon in $TeNiO_3$. The unusual shape of the 4 K isotherm (wasp waist) suggests a metamagnetic transition at very low magnetic fields, lower than 2000 Oe.

Magnetic structure resolution

The magnetic structure resolution was carried out from a set of NPD patterns acquired with $\lambda = 2.42$ Å in the temperature range $2.5 < T < 168.5$ K. Fig. 6 shows the thermal evolution of the NPD patterns, where new peaks of magnetic origin appear at positions forbidden by the space group P*nma*; in particular, new peaks appear at 124 K and below. This implies the establishment of a long-range magnetic order at this temperature, in good agreement with the magnetic measurements. The magnetic structure is defined by the propagation vector $k = 0$, indicating that the magnetic unit cell coincides with the chemical one. For the resolution of the magnetic structure, the possible solutions compatible with the

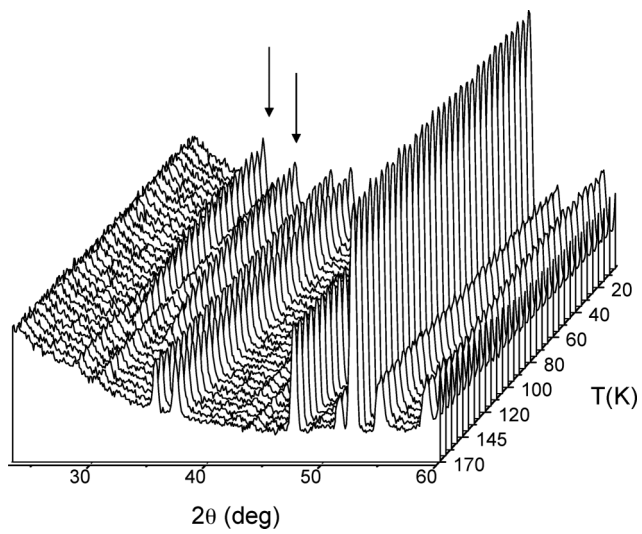

Fig. 6 Thermal evolution of the NPD patterns collected with $\lambda = 2.42$ Å. The arrows indicate the (110) and (011) magnetic reflections.

crystallographic structure for $k = 0$ have been determined using the Basireps program included in the FULLPROF suite.[9] After checking the different solutions, the magnetic structure that shows the best agreement with the experimental data for $TeNiO_3$ corresponds to the magnetic mode G_yF_z. This mode specifies that the magnetic moments are oriented along the y-direction, with a canting along the z-axis. This ferromagnetic component explains the weak FM observed in the magnetization isotherms. Fig. 7 shows the good agreement between the observed and calculated NPD patterns after refinement of the magnetic structure at $T = 2.5$ K. At this temperature, the ordered magnetic moment for the Ni^{2+} ions is 1.88(5) μ_B for the G_y mode and 0.9(2) μ_B for the F_z mode. The thermal variation of the magnetic moment of Ni^{2+} is displayed in Fig. 8. The ordered magnetic moments increase monotonically below T_N and reach saturation at low temperature. There is no anomalous variation at $T = 40$ K that could account for the inflexion in the susceptibility shown in Fig. 4. A view of the magnetic structure is displayed in Fig. 9. The magnetic structure can be described as an antiferromagnetic arrangement of Ni^{2+} moments lying along the b-direction, with a significant canting along the c-direction. Fig. 10 shows the thermal evolution of the unit cell parameters and the volume of $TeNiO_3$. A contraction is observed when the temperature decreases across the temperature range $2.3 < T < 168.5$ K, although the evolution is less significant below ≅100 K, probably due to magnetostrictive effects.

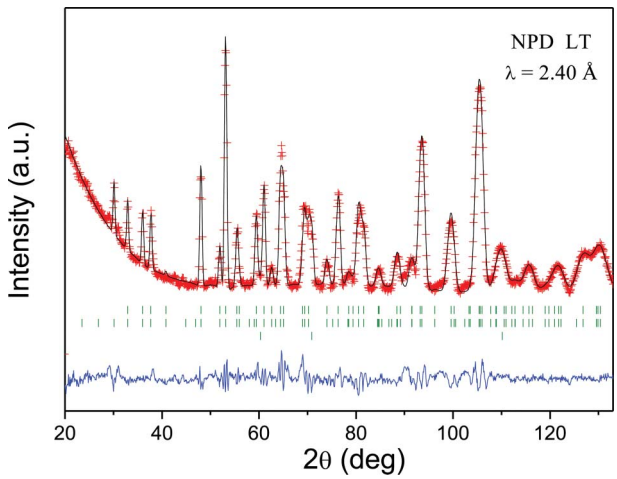

Fig. 7 Experimental (crosses) and calculated (solid line) NPD patterns collected with $\lambda = 2.42$ Å at $T = 2.5$ K for $TeNiO_3$; the first and third series of tick marks correspond, respectively, to the nuclear and magnetic Bragg reflections of $TeNiO_3$, and the second to the nuclear peaks of NiO.

Discussion

$TeNiO_3$ crystallizes in an orthorhombic superstructure of perovskite, with unit cell parameters verifying the relationship $b/\sqrt{2} > c$ (P*nma* setting), which corresponds to the so-called O-orthorhombic distortion of perovskite. The moderate ionic size of the Te^{4+} ion (0.97 Å in six-fold coordination[10]) gives rise to a considerable tilting effect of the NiO_6 octahedra in order to optimize the Te–O distances, with Ni–O–Ni angles (ϕ) in the range 129.6–133.7° (Table 2), which are abnormally small for perovskite-related structures. The average tilting angle, estimated

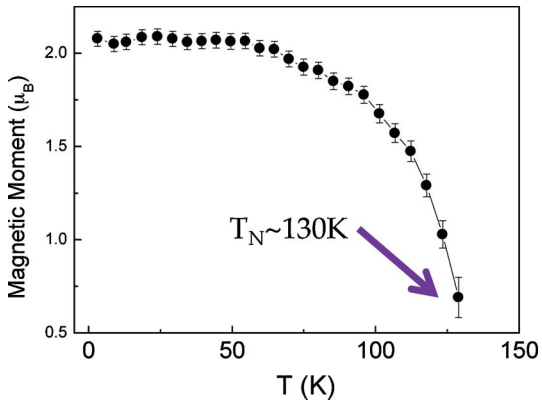

Fig. 8 Thermal evolution of the ordered Ni^{2+} magnetic moments after refinement of the magnetic structure from sequential NPD data.

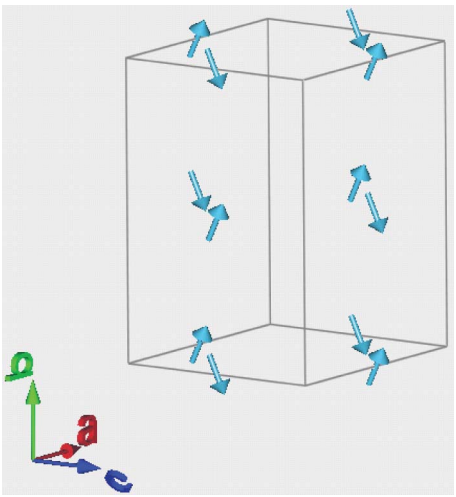

Fig. 9 A schematic view of the magnetic structure of $TeNiO_3$ (only the Ni moments are displayed).

as $\varphi = (180 - <\phi>)/2$, is 24.17°. This is slightly smaller than that observed for $SeNiO_3$[7] (of 25.6°) as it corresponds to the larger ionic size of Te^{4+} *vs.* Se^{4+}.[10] The strong tilting effect drives a deformation of the Te coordination environment; in fact, Te shows 3 short bonds to oxygen atoms at 1.92 Å and 5 long bonds in the 2.69–2.90 Å range. This observation suggests that the Te^{4+} ions form strong covalent bonds with 3 out of the 8 surrounding oxygen atoms, configuring $(Te–O_3)^{2-}$ polyhedra in a trigonal pyramidal configuration with O–Te–O angles between 93–101° (Table 2). The oxygen coordination environment of Te, with three short bonds to O1 and two O2 oxygen atoms, is displayed in Fig. 11. The observed irregular environment is driven by the presence of the Te^{4+} non-bonded lone $4s^2$ electron pair, which should be directed towards the apex of each trigonal pyramid, as suggested in the figure. Similar trigonal environments have also been observed for $SeMO_3$ (M = Mn, Ni, Co, Cu).[1,6,7] Very probably, the formation of the previously mentioned very covalent Te–O bonds is an important ingredient in the stability of $TeNiO_3$ perovskite. It is worth mentioning that Woodward[11] previously indicated that the importance of covalent A–O bonding interactions increases with the electronegativity of the A cation in ABO_3 perovskites, which drives the further stabilization of the $a^+b^-b^-$ tilt system (the one defined in the space group P*nma*).

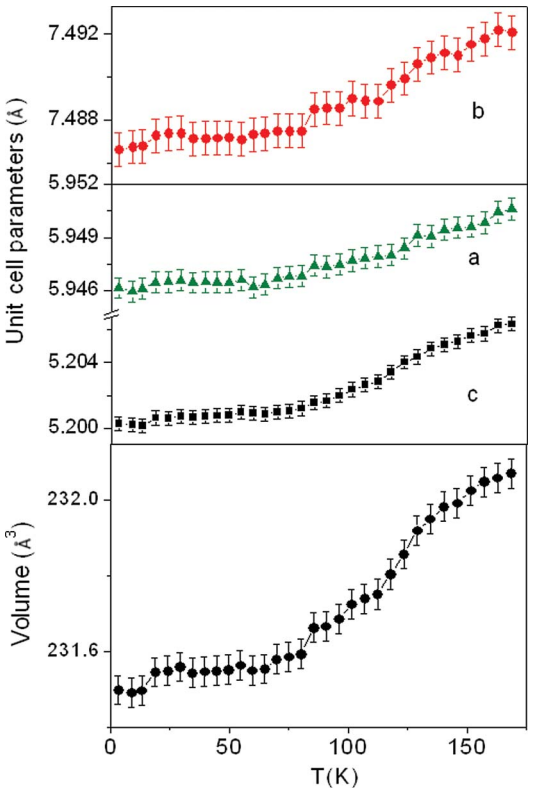

Fig. 10 Thermal evolution of the unit cell parameters and volume of $TeNiO_3$.

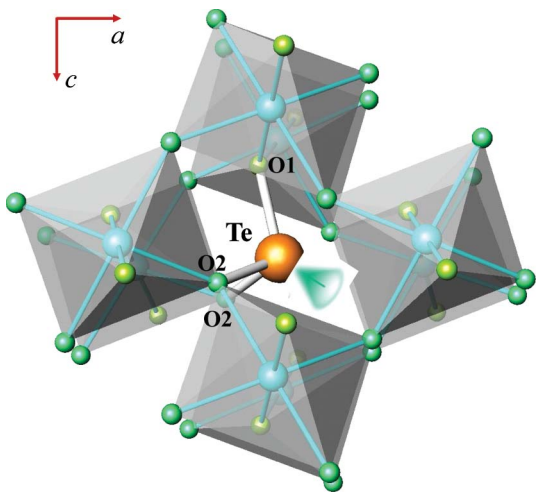

Fig. 11 View of the irregular Te coordination environment with three short bonds to O1 and two O2 oxygen atoms; the direction of the electron lone pair is suggested.

The NiO_6 octahedra are not regular but show short, medium and long Ni–O distances of 2.073(2), 2.098(3) and 2.208(3) Å. This situation may seem reminiscent of the bond length distribution observed in manganese perovskites, $RMnO_3$, where alternating short–long Mn–O distances occurring in the basal plane have been explained as a function of the orbital ordering of the two e_g orbitals; only one of them being occupied by an electron. This distortion can be quantified with the Δ_d parameter, concerning the deviation of Ni–O distances with respect to the average

<Ni–O> value, defined as $\Delta_d = (1/6)\sum_{n=1,6}[(d_n - <d>)/<d>]^2$. For $TeNiO_3$, Δ_d is 7.61×10^{-4}, which is comparable to the values obtained for Se perovskites, *e.g.* $SeNiO_3$ and $SeMnO_3$ of 2.96×10^{-4} and 3.71×10^{-4}, respectively. In any case, all of these figures are significantly smaller than those observed for $RMnO_3$ perovskites, where the Jahn–Teller character of Mn^{3+} originates a dramatic electronic-driven distortion; for instance $\Delta_d = 49.7 \times 10^{-4}$ for $DyMnO_3$.[12] In the present case, $TeNiO_3$ contains Ni^{2+} with a non-Jahn–Teller electronic configuration of $t^6_{2g}e^2_g$: the relatively small octahedral distortion is driven by steric effects, given the small size of Te^{4+} ions occupying the A sites of the perovskite structure.

$TeNiO_3$ shows an antiferromagnetic ordering below $T_N \approx 130$ K; the magnetic structure investigated from low-temperature NPD data corresponds to a G_yF_z mode describing a canted arrangement of the antiferromagnetically-coupled Ni^{2+} magnetic moments. The magnetic unit cell coincides with the chemical one ($k = 0$) and the magnetic structure remains stable down to 2.5 K. The change in the slope observed in the susceptibility curve (Fig. 4) at 40 K could be related to a metamagnetic transition induced by the magnetic field. These transitions occur in antiferromagnetic systems where the spontaneous antiferromagnetic interactions are weak in nature, and the long-range antiferromagnetic structure can be destroyed by the application of an external magnetic field; they correspond to a spin-flop transition from an AF state to a ferromagnetically-polarized spin state.[13] It is important to remark that the neutron data collected at $H = 0$ are not able to detect the apparent change of the magnetic arrangement suggested by the increase in the magnetization in the susceptibility curve below 40 K. This result confirms that this susceptibility anomaly is not accompanied by a change in the long-range ferromagnetic ordering of the Ni spins.

The determined magnetic structure (G_yF_z) accounts for the weak ferromagnetism effect observed in the magnetization isotherms below T_N (Fig. 5). The application of an external magnetic field probably enhances the ferromagnetic component, explaining the relatively high remnant magnetization of 0.05 μ_B observed at 4 K (Fig. 5). The infrequent shape of the magnetization isotherms, on the other hand, is also symptomatic of a metamagnetic transition, as mentioned above. The ordered magnetic moment for the Ni^{2+} ions is 2.08(5) μ_B, close to that expected for spin-only Ni^{2+}cations with the configuration $t^6_{2g}e^2_g$ (2 μ_B per Ni^{2+} ion). It is worth comparing the ordering temperature with that of the closely related compound $SeNiO_3$, with $T_N \approx 104$ K.[7] The superexchange interactions are clearly stronger in $TeNiO_3$, with $T_N \approx 130$ K. There is a two-fold effect that accounts for this observation. On the one hand, the smaller tilting angle of the NiO_6 octahedra (average Ni–O–Ni angle of 129° for A = Se and 131.7° for A = Te) improves the O 2p–Ni 3d orbital overlap, even though the average Ni–O distance of 2.114 Å is shorter in $SeNiO_3$ *vs.* 2.126 Å for $TeNiO_3$. On the other hand, the lower electronegativity of Te *vs.* Se results in more weakly covalent Te–O bonds *vs.* Se–O bonds and concomitantly allows the electron cloud to shift towards the Ni–O bonds through common oxygen atoms across Te–O–Ni paths, thus additionally strengthening and enhancing the O 2p–Ni 3d orbital overlap and promoting the antiferromagnetic superexchange interactions in $TeNiO_3$.

Conclusion

$TeNiO_3$ presents an O-orthorhombically distorted perovskite structure, where the strongly tilted NiO_6 octahedra show an average rotation angle of 24.17°. The TeO_8 polyhedra are extremely distorted due to the presence of the electron lone pair of Te(IV), giving rise to effective $(TeO_3)^{2-}$ polyhedra; the covalent Te–O bonds contribute to the stability of the $a^+b^-b^-$ tilt system of the NiO_6 octahedral network. The NiO_6 octahedra are also axially distorted, although the octahedral deformation is one order of magnitude smaller than that observed in $RMnO_3$ perovskites. The magnetic structure observed below $T_N \approx 130$ K is defined by a propagation vector $k = 0$ and the basis vector $(0,G_y,F_z)$. It is a non-collinear antiferromagnetic arrangement of Ni^{2+} spins lying along the y-direction and canted along the z-direction. The symmetry of the magnetic structure accounts for the weak ferromagnetism effect observed in the magnetization isotherms. For the Ni^{2+} ions, the magnetic moment at $T = 2.5$ K is 2.08(5) μ_B, which is compatible with the ground state electronic configuration $t^6_{2g}e^2_g$ ($S = 1$).

Acknowledgements

We acknowledge the financial support of the Spanish Ministry of Science and Innovation to the project MAT2010-16404. We are grateful to ILL for making all facilities available. We thank Dr M. García-Hernández for carrying out the magnetic measurements.

References

1 K. Kohn, K. Inoue, O. Horie and S. Akimoto, *J. Solid State Chem.*, 1976, **18**, 27.
2 M. A. Subramanian, A. P. Ramirez, W. J. Marshall and Phys, *Phys. Rev. Lett.*, 1999, **82**, 1558.
3 T. Kimura, S. Kawamoto and I. Yamada, *Phys. Rev. B: Condens. Matter Mater. Phys.*, 2003, **67**, 180401.
4 G. Lawes, A. P. Ramírez, C. M. Varma and M. A. Subramanian, *Phys. Rev. Lett.*, 2003, **91**, 257208.
5 R. Escamilla, A. Durán, M. I. Rosales, E. Morán and M. A. Alario-Franco, *J. Phys.: Condens. Matter*, 2003, **15**, 1951.
6 A. Muñoz, J. A. Alonso, M. J. Martínez-Lope, E. Morán and R. Escamilla, *Phys. Rev. B: Condens. Matter Mater. Phys.*, 2006, **73**, 104442.
7 A. Muñoz, J. A. Alonso, M. J. Martínez, H. Falcón, M. García and E. Morán, *Dalton Trans.*, 2006, 4936.
8 H. M. Rietveld, *J. Appl. Crystallogr.*, 1969, **2**, 65.
9 J. Rodríguez-Carvajal, *Phys. B*, 1993, **192**, 55.
10 R. D. Shannon, *Acta Crystallogr., Sect. A: Cryst. Phys., Diffr., Theor. Gen. Crystallogr.*, 1976, **32**, 751.
11 P. M. Woodward, *Acta Crystallogr., Sect. B: Struct. Sci.*, 1997, **53**, 44.
12 J. A. Alonso, M. J. Martínez-Lope, M. T. Casais and M. T. Fernandez-Díaz, *Inorg. Chem.*, 2000, **39**, 917.
13 J. L. Luo, N. L. Wang, G. T. Liu, D. Wu, X. N. Jing, F. Hu and T. Xiang, *Phys. Rev. Lett.*, 2004, **93**, 187203.

